Image-based deformation measurement

Marco Scaioni · Tiantian Feng · Luigi Barazzetti · Mattia Previtali · Riccardo Roncella

Received: 26 March 2014 / Accepted: 10 December 2014
Published online: 28 December 2014

M. Scaioni (✉) · T. Feng
College of Surveying and Geo-Informatics, Tongji University,
1239 Siping road, Shanghai 200092, People's Republic of China
e-mail: marco.scaioni@polimi.it

T. Feng
e-mail: fengtiantian@tongji.edu.cn

M. Scaioni · L. Barazzetti · M. Previtali
Department of Architecture, Built Environment and Construction Engineering, Politecnico di Milano, via Ponzio 31,
20133 Milan, Italy

L. Barazzetti
e-mail: luigi.barazzetti@polimi.it

M. Previtali
e-mail: mattia.previtali@mail.polimi.it

R. Roncella
Department of Civil, Environmental, Land Management Engineering and Architecture, University of Parma, via Parco Area delle Scienze, 181/a, 43124 Parma, Italy
e-mail: riccardo.roncella@unipr.it

Introduction

The analysis of deformations and geometric changes of vari-ous kinds of objects is relevant to many fields of geosciences and engineering. Measurement is a main task in this process, which can be afforded by using several techniques and sensors. It is out of the scope of this paper to give an exhaustive review on this topic, spanning from the investigation of crustal deformations in geodynamics to microscopic observations in nanomaterial science. Moreover, several different platforms are used, including close-range sensors, unmanned aerial vehicles (or UAVs), manned aircrafts, and satellites. For this reason, we limit the topic on applications where ground-based cameras are used for capturing images of objects at a distance ranging from few decimeters to about 500 m.

Generally speaking, the use of imagery as data source for measurement can feature several important advantages: the storage of a huge quantity of information, the simpler understanding and interpretation with respect to laser point clouds or single point observations, the possibility of off-line measurements, and the non-contact with the object.

Close-range photogrammetry (CRP), which is the science dealing with the measurement and 3D reconstruction from

images for *non-topographic* applications (see Luhmann et al. 2013), became relevant to *deformation measurement* (DM) and image metrology with the advent of the so-called *analytical* techniques. Although CRP was still based on analogue film photos, the photogrammetric reconstruction relied on the acquisition of numerical values of point coordinates thanks to mono- and analytical stereo-comparators. The precise comparison of precise point coordinates measured on photos taken at different times (or "epochs") started to be a consolidated option. High-quality analogue "metric" and "semi-metric" cameras were specifically designed for CRP, to be widely used up to the end of the 1990s, when they were completely overwhelmed by digital sensors. On the other side, the availability of corresponding image point coordinates gave impulse to a new formulation of the mathematical background of the photogrammetry, including the bundle block adjustment method as the main approach for photogrammetric (or aerial) triangulation (Triggs et al. 2000), the calibration of close-range cameras (Brown 1971), and the design theory of terres-trial photogrammetric networks (Fraser 1996), a term which refers to the organization of camera stations for image acqui-sition. In the era of analytical close-range photogrammetry, the precise measurement (up to 10^{-6}, see Fraser 1992) of signalized points was achieved.

The second important step in the development of DM applications of CRP consists in the success of digital cameras, which progressively took over analogue film cameras since the beginning of the 1990s. The diffusion of digital imagery simplified the data acquisition step and made image processing cheaper: computers and screens replaced comparators. Moreover, the main advantage of *digital photogrammetry* relies on the development of automatic techniques for camera calibration (Fraser 2013), image orientation (Remondino et al. 2012), and 3D surface reconstruction (Grün 2012). Along with the diffusion of digital cameras, image processing and computer vision communities have made a great contribution to CRP, see Hartley and Zissermann (2006) and Szelisky (2010). Today photogrammetry, image processing, and computer vision may largely benefit from one another.

When dealing with the state-of-the-art CRP, the first aspect to be considered is related to cameras, which are used for the acquisition of optical images. The selection of one specific sensor mainly depends on the sensor format and resolution, the sensor type (CCD, CMOS, Foveon), and the stability over time (Luhmann et al. 2013). This topic has been recently discussed in Scaioni et al. (2014a).

Every digital camera has to be calibrated to reconstruct the internal geometry (inner orientation—IO) and to model lens distortions, see Luhmann et al. (2013) and Fraser (2013). This task, which is today well assessed and consolidated in CRP, allows the application of standard digital cameras for metric purposes. Calibration may be accomplished by the user beforehand or just after image acquisition. A set of calibration parameters may have a limited temporal validity. Thus, a periodic repetition of the calibration should be considered, for example, at monthly intervals or after any events that could influence the calibration setup (e.g., long trips, the use in harsh environment, etc.).

Depending on the geometry and the size of the target object, a variable number of images have to be repeatedly captured at any observation epochs. Image exterior orienta-tion (EO) refers to the reconstruction of the position and attitude of any camera poses with respect to a ground refer-ence system (GRS) where the object has to be rendered (Luhmann et al. 2013). This operation can be easily afforded using fully automatic approaches that are now implemented into low-cost software packages (e.g., iWitness Pro®, PhotoModeler®, PhotoScan®, and others), see Remondino et al. (2012). In the case higher precision or reliability is required, some coded targets (see "Applications based on coded targets") can be installed on the object to assist auto-matic EO process, but also markerless approaches are today fully operational.

Image-based deformation measurement (IBDM) techniques may be organized into three main categories:

1. Measurement of 2D or 3D displacements of specific points on the surface of an object by installing coded targets, see "Applications based on coded targets";
2. *Surface-point tracking* (SPT) in 2D or 3D: these methods can also track points on the object surface, but here a much denser field of tracked points may be obtained thanks to image matching algorithms, see "Surface-point tracking";
3. *Comparison of 3D surfaces* reconstructed from at least two images gathered in correspondence of any observa-tion epochs. Surfaces are reconstructed by using dense image matching techniques, see "Surface comparison."

Although applications in category (1) are used for high-precision metrology where pointwise measurements are needed, categories (2) and (3) are more focused on providing observations over full areas (area-based deformation measurement—ABDM). Such techniques are important for studying those processes where single points are not enough to completely describe the phenomenon under investigation, or the point signalization is difficult or even impossible (e.g., with very small objects). Moreover, where pointwise measure-ments are planned to monitor specific points in well-defined locations (by using photogrammetry or geodetic techniques), ABDM may give an overview on the remainder portions of the object surface. Such techniques do not only comprehend image-based approaches but also entail 3D scanning (Vosselman and Maas 2010), 3D imaging sensors (Remondino and Stoppa 2013), and ground-based synthetic

aperture radar (or GBSAR) sensors, see Monserrat et al. (2014).

The use of efficient visualization techniques is quite im-portant for the presentation of results of any IBDM process. Indeed, when synthetic properties or displacements of a few control points have to be displayed, traditional 2D plots (see, e.g., Fig. 7) may give an exhaustive outlook on what happened during the observation period. On the other hand, when ABDM is operated, the displacement field requires the use of more efficient and illustrative static and dynamic visuali-zation tools. In the static category, the visualization through vector displacement graphics overlapped to a picture of the object (see Figs. 2 and 5) and displacement maps (see Figs. 9 and 10) are quite effective tools. The dynamic category com-prehends animations and videos that may offer an immediate idea of the process development (Mortenson 1985; Hoffmann 1989).

This paper gives an overview of the different approaches for IBDM organized in the categories exposed above ("IBDM methodologies"). "Review of IBDM applications" reports some examples coming from the experience of the authors. Eventually, "Conclusions" draws some conclusions.

IBDM methodologies

Applications based on coded targets

This section will briefly review the applications based on coded targets, being this a standard and consolidated approach which is also widely covered in books (see, e.g., Luhmann et al. 2013). On the other hand, some aspects may also hold for applications in "Surface-point tracking" and "Surface comparison." For this reason, they are recalled here.

Generally, a project should start with the definition of points to track over time. In correspondence of each point, a *target* is fixed to remain stable during the whole period of observation. A target is usually made up of a dark symbol on a light background (or vice versa), which can help automatic recognition and measurement in the images (see Fig. 1). Also *color targets* are commonly adopted. The target may also include a "coded" symbol (coded target) that is used for labeling (see Fig. 1), e.g., to link corresponding targets in different images. Alternatively, point labeling can be done manually.

Fig. 1 Examples of different types of coded targets

The EO scheme depends on the camera setup. If cameras are fixed (like in lab experiments), the EO can be established beforehand. In the case the sensors are repositioned at each epoch, some targets need to be set up in stable positions to fix the GRS. This solution is suggested to assess the stability also in the case the sensors are fixed. In Scaioni et al. (2014a) study, the use of some targets as ground control points (GCPs) is discussed. Three-dimensional coordinates of GCPs need to be determined independently, for example, by means of geodetic techniques. They allow one to completely set up the spatial datum of each photogrammetric network and to compare other control points by subtracting their absolute coordinates measured at different epochs. However, in many cases, only relative variations are needed, which do not call for the setup of a full 3D datum. As is shown in the examples at "Multi-station applications", in such cases only the scale has to be fixed, requiring the knowledge of the distance between two targets.

The reconstruction process is purely based on the automatic recognition and measurement of targets' coordinates. Consequently, the precision of final 3D points also depends on the precision of target measurement, which is strictly related to the size of targets. When the size of circular target in the image is large, the effect of eccentricity has to be corrected as discussed in Otepka and Fraser (2004) and Luhmann (2014).

Several *camera configurations* may be adopted. They can be grouped according to the following classification: (a) *single-camera* and (b) *stereo-camera systems* (despite of the name, this configuration is not aimed to obtain stereoscopic vision and cameras may be convergent to improve precision along depth, see Fraser (1996)) and (c) *multi-station networks*. Fixed cameras are commonly used in configurations (a) and (b), while (c) is generally implemented by setting up the same camera at different stations for capturing single shots. However, when the required data acquisition rate is too high to allow the repositioning of the same camera, a fixed multi-camera system has to be established, see the example at "Multi-station applications." Systems made up of three or four cameras are quite popular in such applications.

The selection of the camera configuration mainly depends upon four factors:

1. *Type of displacements* to measure (2D or 3D);
2. *Size of the object* to analyze;
3. Required *measurement rate*; and
4. *Data redundancy*: given that one or two images may suffice for reconstruction in 2D and 3D cases, respective-ly, if the number of images increases, it will benefit the global redundancy of the photogrammetric network (see Fraser et al. 1996).

Single-camera systems are mainly adopted for tracking point displacements during laboratory experiments, for

example, loading tests, see Barazzetti et al. (2010; 2011) and Maas and Hampel (2006). In some cases, if the texture of the surface is uniform, markerless surface-point tracking (SPT) methods described in "Surface-point tracking" cannot be adopted. In such cases, a set of targets has to be deployed to assist the reconstruction of the displacement field. Alternatively, artificial patterns can be painted or projected, see the example at "ABM point-tracking applications." Generally, such systems do not allow for 3D reconstruction, as illustrated in the following sections. On the other hand, when special six degree-of-freedom (6DoF) targets are used, also 3D reconstruction from single-camera systems becomes possible, see Luhmann (2009). An important key-point of single camera systems when measuring high-dynamic processes is the absence of sensor synchronization problems, as discussed in the end of this subsection.

A *stereo-camera* system is needed in those cases when displacements to measure happen in a 3D space. Generally, this configuration is adopted with a pair of fixed cameras, which is the minimal configuration for 3D reconstruction. Cameras always need to be calibrated when used in such class of applications. The geometric model for sensor orientation and object reconstruction can be easily found in the CRP literature.

Generally, the multi-station approach is necessary when a larger surface has to be covered or when a higher precision and controllability with respect to the ones provided by the stereo-camera approach have to be achieved.

The geometric model adopted here is based on the collinearity equations, which establish the relationship between the image and object coordinates of an observed point P_i (in vectors $\mathrm{x_i}=[x_i\ y_i]^T$ and $\mathrm{X_i}=[X_i\ Y_i\ Z_i]^T$, respectively), IO parameters (principal distance c and principal point coordinates x_0 and y_0), and EO of the camera station j (i.e., rotation matrix $\mathbf{R}_\mathrm{j}=[\mathrm{r_{1j}}\ \mathrm{r_{2j}}\ \mathrm{r_{3j}}]^T$ and perspective center vector $\mathrm{X_{0j}}=[X_{0j}\ Y_{0j}\ Z_{0j}]^T$):

$$\begin{aligned} x_i &= x_{0j} + \triangle x - c\frac{\mathrm{r}_{1j}\left(\mathrm{X}_i - \mathrm{X}_{0j}\right)}{\mathrm{r}_{3j}\left(\mathrm{X}_i - \mathrm{X}_{0j}\right)} \\ y_i &= y_{0j} + \triangle y - c\frac{\mathrm{r}_{2j}\left(\mathrm{X}_i - \mathrm{X}_{0j}\right)}{\mathrm{r}_{3j}\left(\mathrm{X}_i - \mathrm{X}_{0j}\right)} \end{aligned} \quad (1)$$

Terms Δx and Δy contain the additional parameters (APs) to correct lens distortion. APs have been evaluated during camera calibration. Also the IO parameters are usually known from calibration and introduced as constants in Eq. (1). As an alternative, the terms Δx and Δy may be set up to 0 if the images have been resampled to output distortion-free images. This option is quite comfortable because it allows the user to completely get rid of lens distortions during successive photogrammetric processing steps. Unfortunately, any resampling of the images may result in low-pass filtering. If a very high precision is needed, the alternative is to apply APs to any image coordinates to compensate for lens distortion.

Image coordinates of point P_i are usually measured on the images, while $\mathbf{R}_\mathrm{j}$, $\mathrm{X_{0j}}$, and the object coordinates of P_i are unknowns to be estimated in a least squares fashion. A system of Eq. (1) is set up to solve for the EO parameters and object point coordinates. A global rank deficiency always exists, which can be fixed by adding some GCPs or using inner constraints, see Granshaw (1980).

When a point can be seen in two images only, as in stereo-camera systems, it gives rise to four Eq. (1). The number of observation equations related to the same point may increase when multiple images are used, resulting in a higher local redundancy and then in a better controllability of the obser-vations, see Grün (1980).

Precision (σ_{XYZ}) of point coordinates in object space can be estimated as proposed in Fraser (1996):

$$\sigma_{XYZ} = \frac{qS\sigma_{im}}{\sqrt{n}} \quad (2)$$

where n is the number of images used for the determination of the point, q accounts for the geometric configuration of the images and may range between 0.4 and 2, S is the average image scale, and σ_{im} is the measurement precision of image coordinates. The relative attitude between the images may influence the precision through factor q in Eq. (2): as is clearly shown in Fraser (1996), the use of convergent images results in a better spatial intersection of corresponding rays which may provide a small and isotropic error ellipses for the recon-structed points.

Today color (RGB) cameras are widely used, with the exception of some metrological applications where industrial mono-chromatic cameras are implemented in permanent data acquisition systems. In target-based applications, colors are not strictly needed to detect targets, unless when special color markers are used (see Fig. 1). If black/white targets are used, target detection may require converting three-channel RGB images into mono-chromatic images. Generally, this task is operated by using weighted combinations of different single colors, but this solution may turn out in a sub-pixel bias when CCD or CMOS sensors are employed. Indeed, the distribution of pixels sensitive to red and blue wavelengths is usually not symmetric in the Bayer scheme that is adopted in most cam-eras (see, e.g., Luhmann et al. 2013). For this reason, the use of the green channel is expected to provide unbiased results due to the symmetric distribution of pixels sensitive to this color.

An important issue to consider when using more than one camera to gather images of a fast developing process is related to sensor synchronization. Indeed, a time misalignment may

lead to use images taken at different times, resulting in errors in the determination of 3D coordinates. Different solutions may be applied if synchronization bias has significant impact, as reported in the literature, see Spencer and Shah (2004) and Raguse and Heipke (2009).

Surface-point tracking

In applications for surface-point tracking (SPT), the attention is focused not only on specific signalized targets but also on the measurement of a dense field of natural features that can be automatically recognized on the surface of the object. Since the early 1980s (see for instance Peters and Ranson 1982), the application of image matching techniques (or digital image correlation, see Goshtasby 2005 and Grün 2012) to strain analysis in material testing has become more and more popular due to the high accuracy that may be achieved, coupled with the full-field description of the material behavior hardly obtainable with other non-contact methods.

If the texture is well contrasted, a dense field of observed points may be detected. In most applications, a single-camera sequence is analyzed (see, e.g., Roncella et al. 2004; Fedele et al. 2014). A fixed station is commonly used, and this turns out in the fact that all the images are already aligned and point displacements are tracked in the same reference frame. On the other hand, if the camera cannot be kept in fixed position, images need preliminary co-registration (see, e.g., Barazzetti and Scaioni 2009). In the case of flat objects, the homography model can be exploited to derive coordinates in object space. In the case of non-flat surfaces, image matching may only give a qualitative output (see the example at "Feature-point tracking applications") but not any metric information. When two (or more) cameras are contemporarily used, corresponding points have also to be found across images taken from different stations. This task is generally more complex because the perspective and radiometric deformations between synchro-nous images have to be taken into consideration.

Several image matching techniques have been developed in the last three decades. Owing to such large number of different implementations, it is quite hard to identify a completely satisfactory taxonomy of the different algorithms, even if very good overviews can be found in the literature (see, e.g., Scharstein et al. 2002 and Baker et al. 2011). Two categories of matching techniques are commonly used: *area-based matching* (ABM) and *feature-based matching* (FBM).

Area-based matching algorithms evaluate the similarity on the basis of image intensity values in the nearby of two approximate corresponding locations on the images. Multi-photo matching techniques may also work with more than two images at the same time. The process starts from a set of "seed" points selected on the first image whose corresponding positions are predicted on the others. ABM algorithms have a pull-in range capability that allows looking for the homologous position also if this is a few pixels far from the predicted location, depending on the specific method.

Feature-based matching algorithms rely on the independent extraction of two sets of features in the images by using *interest operators*, see Jazayeri and Fraser (2010). Depending on the adopted operator (see Table 1), the chance to find several homologous points may be large even if the images differ because of radiometric and geometric deformations. Matching is based on a similarity criterion that also considers a window around the interest points but without any pull-in range capability.

The selection of the matching method depends on the properties of the target object and on the velocity of the image content change. If a slow process is investigated with quite regular changes between consecutive images, ABM has to be preferred (see more details at "Area-based matching for SPT"). If sudden changes may happen, FBM is probably better. Also FBM has to be used when more than one image sequence is used because in such case, the corresponding points have to be recognized in synchronous and asynchronous images. Applications including FBM will be addressed as *feature-point tracking* (FPT) and discussed at "Feature-point tracking."

For general aspects of the photogrammetric process related to sensor orientation and calibration, the same concepts illus-trated in "Applications based on coded targets" still hold. Very often some targets are installed in the scene to help image orientation.

Table 1 Principal *interest operators* adopted in FPT

Operator	Paper	Invariance	Repeatability[a]	Descriptor
Foerstner	Förstner and Gülch (1987)	Rotation, brightness, and contrast	+++	No
Harris	Harris and Stephens (1988)	Rotation, brightness, and contrast	+++	No
SUSAN	Smith and Brady (1997) Lowe	Rotation, brightness, and contrast	++	No
SIFT	(2004)	Scale, rotation, brightness, and contrast	++	Yes
SURF	Bay et al. (2008)	Scale, rotation, brightness, and contrast	++	Yes
FAST	Rosten and Drummond (2006)	Scale, rotation, brightness, and contrast	++	Yes

[a] Repeatability is classified as in Tuytelaars and Mikolajczyk (2008), except for FAST

Area-based matching for SPT

In the sequence of images to analyze, one is selected as reference ("master"). Usually such master is the first one or the central one in the sequence. A grid is set up to locate the points to be tracked using ABM. The grid step depends on the spatial resolution of the desired displacement field. In the hypothesis that images are co-registered, every node of such grid is used as the starting point for matching in the next image. Matching of any single points is carried out independently, even though a filtering stage may occur later to check the consistency of detected displacements of adjacent points. ABM works on the basis of a template extracted around each point on the master. The search is carried out inside a search window extracted around the predicted point in the second image ("slave"). Different matching algorithms can be adopted, but mainly they can be assimilated into the following categories.

Convolution- or correlation-based methods define the dis-placement field as the collection of shifts that yields the best fit to a particular function or yields the optimal value for a partic-ular cost function (e.g., Normalized Cross-Correlation—NCC), see Rosenfeld and Kak (1976). The search window theoretically may span over the whole slave image. In reality, the size and the location of the search window are limited to avoid risk of mismatching in the case of repetitive patterns. Many of these techniques (e.g., NCC), not considering the perspective deformation of the slave with respect to the master image, may find corresponding points only if the local defor-mation inside each window is limited to shifts, while rotation should be smaller than about 5° and scale variation lower than 10 %. NCC may also compensate for a linear radiometric transformation between both images. Precision of these techniques may reach sub-pixel level by applying interpolation of correlation values of the pixels in the nearby of the best solution.

When other deformations than shifts are significant, *locally adaptive methods* such as the Least Squares Matching (LSM) technique can be successfully applied, see Grün (1985). These methods assume that the image (and in some circumstances also the time) domain is continuous or at least differentiable and look for the parameters of a geometric transformation which minimize a cost function including similarity of pixel intensity values and possibly some geometric constraints related to the EO, see Maas (1996). Generally, an affine transformation is implemented in the cost function, but also higher-order geometric transformation can be used if highly localized deformation can be foreseen, see Bethmann and Luhmann (2010) and Roncella et al. (2012). Estimate of linear radiometric transformation can be included into the LSM model, or the preliminary image equalization can be applied, see Forlani et al. (1996). Sub-pixel precision can be directly reached. A template is extracted around each seed points on the master, and the homologous is searched around the predicted position on the slave. In this case, the pull-in range is smaller than with convolution-based techniques, in the order of 1/3 the template size, which usually spans between 15–30 pixels.

Feature-point tracking

In FPT, the search for the homologous points is carried out after extracting a set of features that can be easily distinguished from their neighborhood in any images. Unlike ABM which looks for homologous points around a predicted position on the slave image and then tries to refine it, FBM implemented in FPT simply finds correspondencies in the sets of the extracted features. Generally, the matching stage is applied by exploiting some "descriptors" that are directly worked out by the feature extraction algorithms, see Table 1. Alternatively, other algorithms may extract interesting points and then the matching stage has to be carried out by using an independent measure (usually linear correlation). A thorough taxonomy of different algorithms/techniques can be found in Mikolajczyk and Schmid (2005), Mikolajczyk et al. (2005), and Apollonio et al. (2014).

The major advantage of FPT is the greater *robustness* with respect to ABM methods. This means a larger chance to detect corresponding points in images with different scaling, rotation, and lighting. Consequently, such robustness may be useful to cope with abrupt changes in the scene (see the example at "Feature-point tracking applications"). Another important property of a few operators (see Table 1) is *repeatability*, which refers to the chance to track the same points in a long image sequence.

The typical workflow of FPT is as follows:

1. Image enhancement (optional) by using equalization fil-ters in the case of data sets with poor texture, for example, by Wallis filter (Wallis 1976);
2. Feature extraction: interesting features are independently extracted on both images;
3. Feature-based matching (FBM): each interest point on the master image is compared to any points on the slave. In many applications, some criteria are applied to reduce the searching space and to mitigate the risk of false matching outcomes. In addition, robust outlier rejection methods are usually implemented to get rid of large measurement errors that may occur due to repetitive patterns on the object surface or other motivations, see Barazzetti et al.(2010).

More than one criterion may be also cascaded.

The FPT along with more than two images is done by starting from the set of corresponding points found on the initial two images of the sequence (no. 1 and no. 2). Then,

image no. 2 is considered as the new master and image no. 3 becomes the new slave. The FPT proceeds in this way up to the last image of the sequence.

If a stereo-sequence is considered, points have also to be matched across the images to support the computation of 3D coordinates. Different strategies may be implemented to this purpose, which however are based on the scheme described above. Especially with convergent images, the invariance of the interest operator as well as of the corresponding descriptor with respect to perspective changes is mandatory to allow good feature repeatability and high level of accuracy. In more recent years, many authors documented that basically all the "SIFT-like" point descriptors (see, e.g., Verhagen et al. 2014) may achieve very high level of efficiency, repeatability, and accuracy even with wide baselines and convergent views.

Surface comparison

The use of *dense matching* algorithms (Haala 2013; Remondino et al. 2014) allows computing a *point cloud* to describe the surface of an object. Consequently, two point clouds of the same object gathered at different times may be compared to detect changes and deformations. These may entail (a) rigid-body transformation, (b) loss or accumulation of material, and (c) shape changes.

After camera calibration and image orientation that are accomplished as in the previous cases, dense image matching techniques are applied to provide a set of n point clouds (S_1, S_2,…, S_n) describing the surface of the object at any observa-tion epochs, see "Dense image matching." In a subsequent stage, point clouds are compared among them, see "Techniques for comparing point clouds."

Dense image matching

The aim of dense image matching is to provide a high number of corresponding points in at least two images, which may well approximate the object's surface after spatial intersection. Criteria to use two or more images (stereo or multi-station networks) are the same as described for other categories of applications. Here the starting point is the EO of the images, whose quality is a crucial aspect for dense matching success. An exhaustive description of several existing algorithms is out of the scope of this paper. Readers are addressed to Scharstein and Szeliski (2002), Seitz et al. (2006), Grün (2012), and Remondino et al. (2014). However, we would like to give an outlook on the basic assumptions to which almost all techniques may refer. The presence of repeated patterns, lack of contrast in the images, variation in illuminations, perspective deformations, noise, and also moving objects may significantly affect the results of the matching process. Consequently, image matching strategies that only rely on the similarity between pixel intensity like the ones used for SPT may not be sufficient to cope effectively with these problems. On the other hand, FBM algorithms are not generally suitable for dense matching due to the scarce point density. Technical solutions to deal with the abovementioned problems rely on hierarchical processing, geometric con-straints, and multi-photo matching techniques.

Since Hirschmüller (2005; 2008), Semi-Global Matching (SGM) has largely developed because, thanks to the minimi-zation of a pixelwise cost function, it may better reconstruct fine details and preserve sharp object boundaries, see Dall'Asta and Roncella (2014). In the latest applications, the use of multiple views has been included in SGM to exploit the higher redundancy and the larger information available from more images, see Bethmann and Luhmann (2014).

A last note should be highlighted on the precision of dense matching algorithms. It is difficult to establish some reliable and general reference values due to the extreme variability of operating conditions and image quality on one side and to the lack of exhaustive validation work (Grün 2012) on the other. A safe value of 1–2-pixel precision in image space could be assumed, although some algorithms may reach in good condition sub-pixel results.

Some attempts have been accomplished to compare differ-ent methods, but results obtained so far cannot cover all existing techniques and possible object and network configurations, see Seitz et al. (2006), Remondino et al. (2014), and Toschi et al. (2014).

Techniques for comparing point clouds

Point clouds are usually compared in a pairwise manner. Either a sequential analysis of consecutive pairs of point clouds (S_1 and S_2, S_2 and S_3…, S_{n-1} and S_n) which lead to work out the cumulative deformations or the analysis of any point clouds S_i with respect to a reference point cloud S_r may be followed.

Unfortunately, the reconstructed point clouds are not made up of corresponding points because the surface texture could change in images captured at different epochs, and 3D points computed by image matching may differ. Thus, a direct, "pointwise" comparison is not possible, see Scaioni et al.(2013a). Commonly one method out of the following four categories can be used.

1. For each point of S_i, the closest point in S_r is selected first. Then, the distance between both points is evaluated to obtain the local displacement vector;
2. The reference point cloud S_r is interpolated to derive a continuous digital surface model (DSM). Then, for each point in S_i, the minimum distance with respect to the DSM of S_r is computed and assumed as local displacement vector;

3. Both S_i and S_r are interpolated and corresponding points are established at the nodes of a regular grid (or Digital Elevation Model—DEM). Then, displacements are evaluated along the orthogonal direction to the reference grid after computation of the so called ΔDEM, which is the difference between DEMs derived at both epochs; and
4. Both S_i and S_r are interpolated to derive two DSMs. Then, changes are evaluated by computing the volume comprised between such DSMs.

The selection of one model depends on many conditions and it is difficult to find a ubiquitous solution. Factors that should be considered are expected or prevalent direction of displacements, presence of noise, point density, surface regularity, sharp break-lines, gaps or holes in the data sets, structure of points (2.5D or 3D), magnitude of displacements, and loss/accumulation of material between observation epochs.

A key pre-requisite in the comparison of point clouds is their precise *alignment*, because misalignment errors may strongly affect the final result of ABDM. The typical solution for a correct registration is to establish a stable GRS or to use fixed camera stations during the whole data acquisition. The use of surface comparison can be also carried out by using data from laser scanners (see, e.g., Scaioni et al. 2013a) or other 3D imaging system, see Lichti et al. (2012).

Review of IBDM applications

In this section, selected examples of the application of the methods for IBDM which have been previously described in "IBDM methodologies" are reported. Such examples will give an outlook on the potential capability of IBDM techniques, rather being an exhaustive review of the existing applications. Table 2 resumes the properties of different cameras adopted in the experiments.

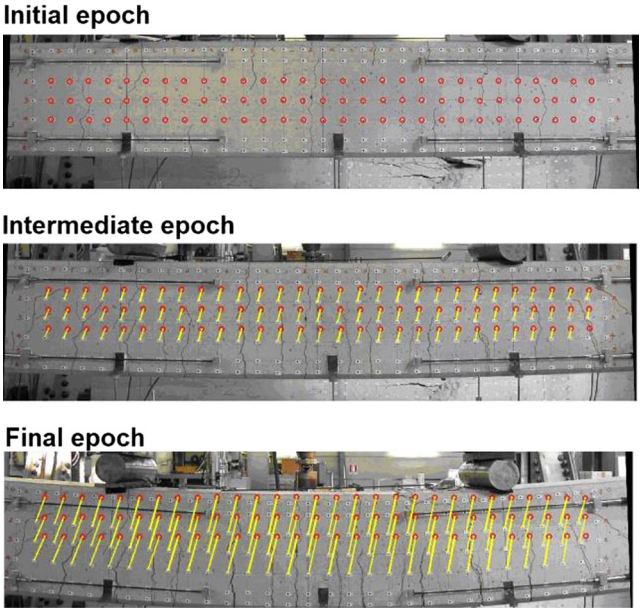

Fig. 2 Measurement of target 2D displacements during a loading test of a reinforced concrete beam (modified from Barazzetti and Scaioni 2010)

Applications with coded targets

Single-camera applications

In Figure 2, a typical application based on a single camera is reported. It concerns the measurement of deformations in a reinforced concrete beam during loading test, see Barazzetti and Scaioni (2010; 2011). A low-cost digital camera was placed at about 130 cm in front of the beam and kept fixed during the experiment. A set of more than 210 circular targets were fixed on the surface, although only the ones in the central part have been tracked along 33 images (variable time interval between 30 s and 2 min). Target size in the images was about 10–11 pixels. Initial positions of targets were found using LSM and a synthetic template as reference. Target positions in the following images of the sequence were also found by using LSM, but this time by using the window extracted around the target in image i to detect the corresponding target in image $i+1$.

Table 2 Technical properties of all cameras adopted in the applications described in this paper

Camera	Type of camera	Sensor	Lens	Sensor size (mm/pixels)	Pixel size (μm)
Nikon D70	SLR	CCD	Sigma 20 mm	23.6×15.8 mm/3008×2000 pix	7.8
Nikon D80	SLR	CCD	Sigma 20 mm	23.6×15.8 mm/3872×2592 pix	6.1
Nikon D200	SLR	CCD	Nikkor 35 mm	23.6×15.8 mm/2896×1944 pix	8.1
Nikon D700	SLR	CMOS	Nikkor 90 mm	36×24 mm/4256×2832 pix	8.4
Basler Pilot piA1600-35gm	Industrial	CCD	Basler 8 mm	11.9×9.7 mm/1608×1308 pix	7.4
Canon EOS 5D Mark II	SLR	CMOS	50 mm	35.8×23.9 mm/5616×3744 pix	6.4

In the application described here, the maximum resolution of Nikon D200 (3872×2592 pix) was not exploited, as described at "Feature-point tracking applications"

The regular pattern of targets and the small displacements between consecutive epochs (max displacement was 81 mm) made quite trivial to assign the same label to corresponding targets. No codes were needed.

It is interesting to notice somehow, under the assumption of completely stable camera, this application could be afforded in the image space. In the end, target coordinates were transformed in the object space using the same homography parameters for any images. This transformation could be computed in the initial image by measuring coordinates of four targets. As image distortion varies in a smooth way in the image and applies the same way to the whole sequence, if displacements between consecutive images are small (a few pixels), its correction may be avoided. The estimated precision of this method depended only on target measurement because other effects did not contribute to relative differences. Generally, a reference value of standard LSM precision may reach up to 1/20-pixel size, although this result has been improved in ideal conditions and with optimized algorithms, see Birgisson et al. (2009). In many applications, worse results may be found as well, depending on the quality of images. We retain that a value about 1/10 pixel is more realistic. In this case, such assumption led to an average precision of $\sigma_{x,y}$= 0.3 mm for the image coordinates. Consequently, the precision of each relative 2D displacement vector was $\sigma_{\Delta s}=\sqrt{2}\ \sigma_{x,y}$= 0.4 mm. Such theoretical results were compared against readings of linear variable differential transformers (LVDTs—see Nyce 2004) located in four different locations. Such analysis, though limited to few points, demonstrated that no significant departures were obtained from both measurement techniques.

Stereo-camera system applications

In the example in Fig. 3 (see Barazzetti and Scaioni 2011 for the details), a small specimen of compacted sand was used to see the effect of a down-scaled foundation model under non-centered loading. This resulted in a 3D rotation of the model, which could not be evaluated using traditional linear displace-ment or inclination sensors. Moreover, the limited size of the specimen resulted in several problems with the installation of contact sensors. Thus, two cameras Nikon D70 were placed at a distance of about 55 cm from the object using a baseline (i.e., the distance between both cameras) of 50 cm. A set of targets were placed on the different parts of the trial device, in order to detect also any relative displacements in the whole structure. Also 3D rotations between consecutive epochs were detected by using the 3D reconstructed coordinates of all targets on the small foundation.

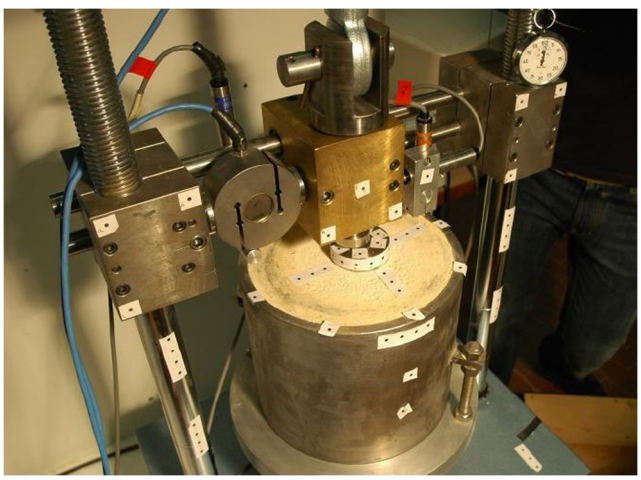

Fig. 3 Specimen of compacted sand under loading of a foundation model (modified from Barazzetti and Scaioni 2011)

In this application, no coded targets were used because of the small specimen size. Targets were automatically measured in any images of the stereo-sequence by LSM. Labeling was done manually in the first image pair. Then, because of the small displacements between consecutive images, labeling of targets was automatically done by exploiting the proximity of image coordinates with respect to previous scenes. The low speed of the experiment did not result in any problems with camera synchronization.

Results showed a theoretical accuracy of ±0.02 mm in the measurement of target displacements, whose average size in the images was 0.6 pixels. This result is consistent with the theoretical accuracy obtainable with the hypothesis of images in the "normal" configuration, see Luhmann et al. (2013).

Multi-station applications

Two examples are reported for multi-station applications. In the first one (see Scaioni et al. 2014b), the aim was to measure deformations of tunnel cross-sections. For this purpose, a set of targets was fixed on the vault thanks to special supports (see Fig. 4). Then, at each epoch, a block of four images was captured using a Nikon D700 camera. This technique had the drawback of requiring the independent measurement of a distance between two targets close to the pavement for setting the scale at any observation epochs. A graduated wire was adopted to this aim. Other components of the 3D datum were not constrained, because only relative inter-distances between couples of targets were needed.

Three-dimensional coordinates of targets measured during the first observation epoch (t_0) were assumed as reference. Because targets were positioned to approximately lie in a vertical plane, the equation of this plane was estimated and coordinates of any targets projected onto this reference surface. This allowed splitting the deformation analysis in two parts: "off-plane" displacements, which could be evaluated at each epoch as residuals with respect to the interpolating plane, and "in-plane" displacements. An affine transformation could

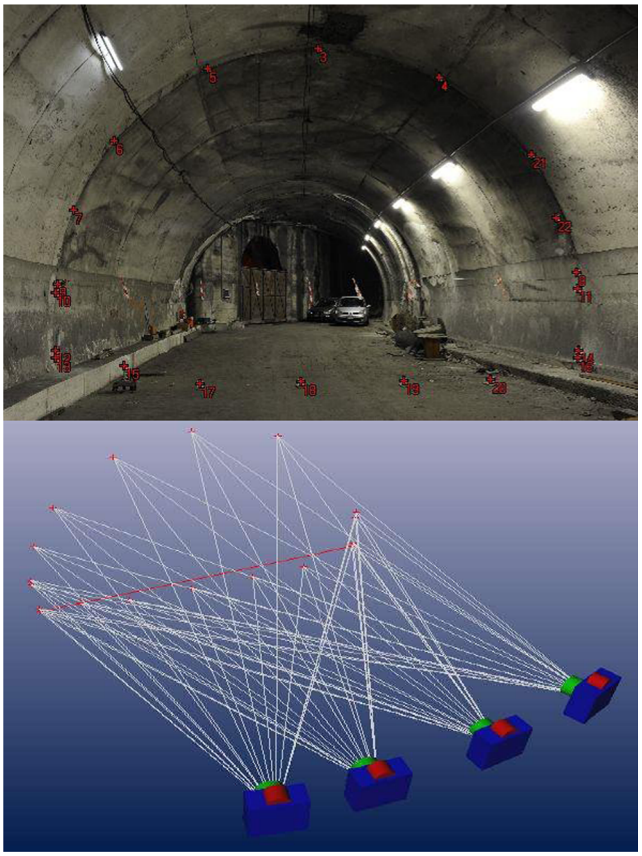

Fig. 4 Example of a multi-station IBDM system adopted for monitoring deformation in tunnel cross-sections. On the *top*, the target setup is shown. On the *bottom*, the photogrammetric network scheme is shown

be used to transform the coordinates of targets at the generic epoch t_i into the reference system of epoch t_0. Coefficients of the affine transformation were estimated by considering any pairs of corresponding targets at both epochs. A robust L1-norm estimate allowed reducing the influence of individual target displacements or measurement errors.

Once all parameters a_{jk} of the affine transformation have been estimated, in-plane displacements of each target could be analyzed.

Experiments with simulated target displacements demonstrated the chance to achieve a theoretical accuracy of ±0.5 mm. After comparison with high-precision geodetic observations, the accuracy of the real photogrammetric measurements was evaluated to be consistent with the theoretical one and resulted in about 0.2-pixel.

The second example reports about an application for measuring deformation on the surface of an ancient masonry wall during in situ loading test in the basement of Istituto Lombardo (Milan, Italy—see Barazzetti and Scaioni 2011). The experiment setup is shown in Fig. 5. Four cameras Nikon D80 were placed in front of the area where an artificial compression was induced using bolted steel plates. Multi-station photogrammetry was necessary because of the high precision required, especially for detecting possible off-plane deformations with respect to the wall surface. The standard procedure for measuring deformations during such tests is to install a set of LVDTs, which may provide information only on a limited number of locations. Moreover, LVDTs cannot observe off-plane displacements.

Cameras had been independently calibrated before the experiment. Shooting was synchronized among different cameras and with the control unit of the loading device and LVDTs. Also in this case, the slow deformation speed did not entail any problems related to sensor synchronization. EO parameters of all camera stations were computed before the loading test started. Some coded targets (see Fig. 5 on the right) were positioned to this purpose. The EO was assumed to be unchanged at any epochs, in the hypothesis that no movements occurred to camera stations. Some non-coded targets were glued on the central area of the specimen to track the displacements.

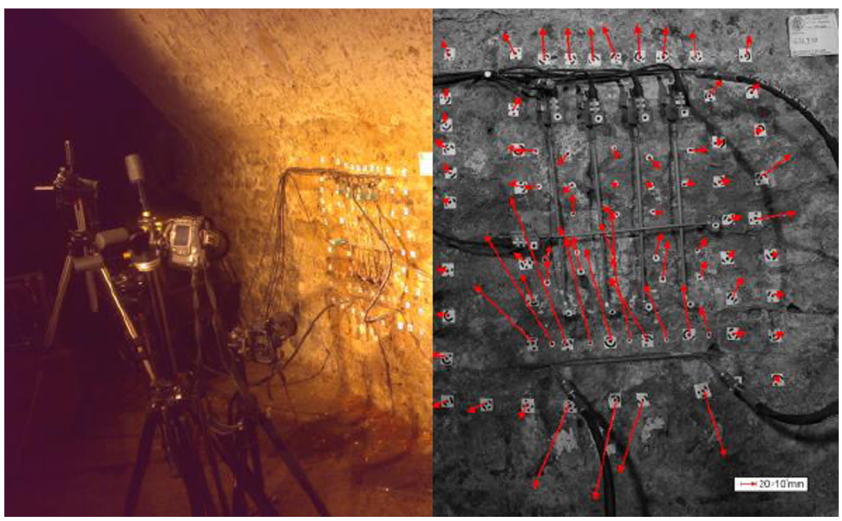

Fig. 5 Multi-station camera system (on the *left*) adopted for measuring deformation (on the *right*) during a loading test of an ancient masonry wall (Istituto Lombardo, Milan, Italy)

Theoretical accuracies of ±0.008 and ±0.013 mm were found for in-plane and off-plane displacements, respectively. These values are comparable with the pixel resolution re-projected onto the wall, i.e., 0.1-pixel. The improvement obtained is also due to the robust configuration of the network including convergent images.

Applications based on SPT

ABM point-tracking applications

A SPT analysis to evaluate the cracking response of a polymer-modified asphalt binder is presented. The cracking behavior of the mastics was investigated using a modified Direct Tension Test (Niu et al. 2014) developed at the University of Parma, Italy. In particular, the analysis was focused on a very small 10-mm-wide dog bone specimen (see Fig. 6), and the results were used to calibrate and validate a finite element method (FEM) numerical model.

For image acquisition, a Basler Pilot piA1600-35gm camera equipped with 8-mm lens was used. Due to the very small region of interest (ROI) depicted in Fig. 6, it was rather impossible to apply coded target on the surface of the specimen. At the same time, a very detailed (i.e., with many measurement locations) description of the strain field was required to correctly validate the numerical model. The ABM approach was then considered the best solution. A grid with 0.2-mm steps was established to fix the initial positions of LSM. To improve the contrast of the material texture and to achieve the highest level of accuracy in SPT, a talcum spray treatment was applied to all the specimens.

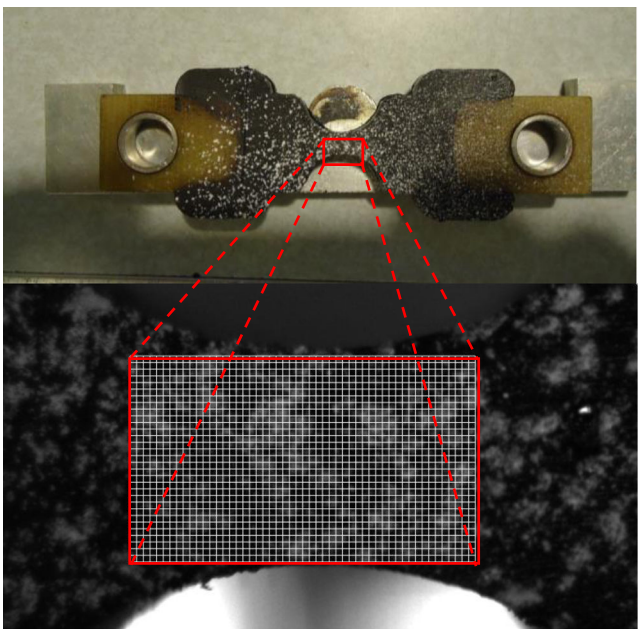

Fig. 6 One of the polymer-modified dog bone specimen used in the ABM-SPT analysis described at "ABM point-tracking applications"

The test is usually very fast to avoid unwanted viscous behavior of the mastic. The speed of the loading frame is set to induce cracking initiation in approx. 1–2 s. For this reason, only the central part of the camera sensor was used to acquire images (ROI of 1608×500 pixels) achieving a standard frame rate of 80 frame per second (fps).

In Fig. 7, the comparison of the results with the numerical model simulation is presented for one of the mastics. Axes report stress and relative strain along x and y directions, respectively. The FEM model assumes an elastic behavior for the material and thus can be com-pared only for the first part of the test. The reported example shows a maximum departure between the mea-sured (in blue, labeled "strain") and simulated (in red, labeled "sim-strain") values of 0.8 % with an overall standard deviation (for the linear part) of 0.4 %. The analysis of the graph can clearly identify the precise moment of crack initiation and of the material resistance failure, as well as the elastic response of the crack edges.

Feature-point tracking applications

As an example of this category, the analysis of two image sequences gathered by means of Nikon D200 cameras is shown. The object is represented by a landslide simulation facility during experiments established at Tongji University, Shanghai (P.R. China), see Scaioni et al. (2013b). FPT is used to highlight the region where the sliding process started in order to predict a forthcoming collapse on the basis of number and velocity of tracked points. Since the physical phenomenon is not continuous, FPT is restarted by considering all interest points found in every image of the sequence and matched with the following one.

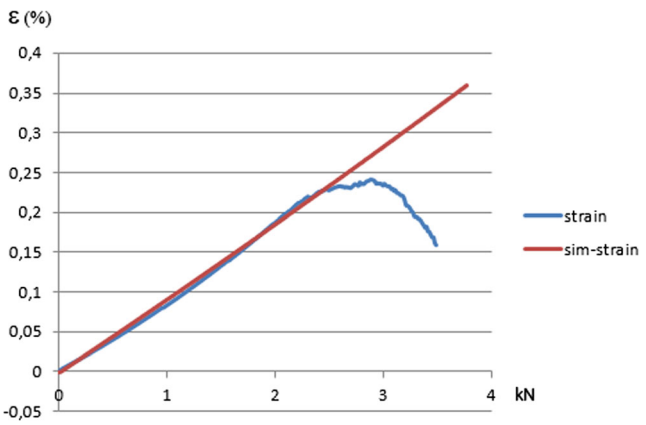

Fig. 7 Stress-strain diagram of experimental (in *blue*) and theoretical (in *red*) results in the experiment described at "ABM point-tracking applications"

This solution has allowed either tracking those points that were continuously moving in more images as well as detect-ing sudden and discontinuous displacements. FBM has been implemented by using SURF, which may provide slightly less interest points than SIFT, but with a smaller computational cost. This choice has been motivated by the need of designing a prototype system to deal with real-time monitoring of full-scale landslides, see Feng et al. (2012).

Some results of FPT are displayed in Fig. 8. As can be seen, the surface of the down-scaled slope is not flat and FPT cannot provide metric results. On the other hand, the availability of the sequence gathered by a second camera forming a stereo-camera system may also provide 3D coordinates of points. In that case, points should be also match across any synchronous image pairs.

The aim of this experiment was to detect precursory events of small and large slope collapses. The three columns of Fig. 8 show the images just before (in the upper row) and after (in the lower row) three failures. The time elapsed between two consecutive images was 30 s. As it can be seen in the figure, feature points (in green) were tracked in the sequence just before a col-lapse, then they were lost. The analysis of number (reported in the first row), extension, and velocity of tracked points could be used to infer potential collapses.

Theoretical evaluation of point precision in object space provided superior limit values of approx. ±1 mm in the plane parallel to the sensor and approx. ±5 mm along depth (see Scaioni et al. 2014a). The speed of deformations did not entail significant effects due to camera synchronization errors. Since the aim here was chiefly to obtain qualitative information on the tracked point distribution, validation measurements were not available.

Applications based on surface comparison

A permanent stereo-camera system

A quite innovative application of DSM comparison in IBDM is described in Roncella et al. (2014) where the displacements of a landslide in the Italian Alps are evaluated through the use of a fixed photogrammetric stereo-camera system. Two fixed remote stations on the opposite flank of the valley, approx. 500 m from the slope, periodically record (usually one frame per hour) images of the landslide area and send them to a central processing unit that, through automated dense matching algorithms, produce the DSM of the entire slope. A couple of 21-megapixel Canon EOS 5D Mark II cameras equipped with 50-mm lens are used. Geometrically constrained LSM is implemented to find corresponding points: in addition to the evaluation of similarity between intensity values, also the epipolar constrain is exploited. Due to landslide visibility limitation, the baseline between the two camera stations is quite small (approx. 100 m) if compared with the distance from the object. Consequently, the precision of 3D coordinates of object points is unsatisfactory for short monitoring periods: in the farther part of the slope, precision up to 10 cm in depth direction should be expected, and the system cannot be used, for instance, as an alert device to highlight sudden landslide accelerations. Nonetheless, thanks to its very low cost, the system can be used for minor (and less dangerous) landslide monitoring over a long period, giving important pre-alerting information.

The lesson learnt from this experience chiefly consists in the great attention to be paid in the system design, since both imaging geometry and illumination might change during the monitoring period that could also span over several years. At

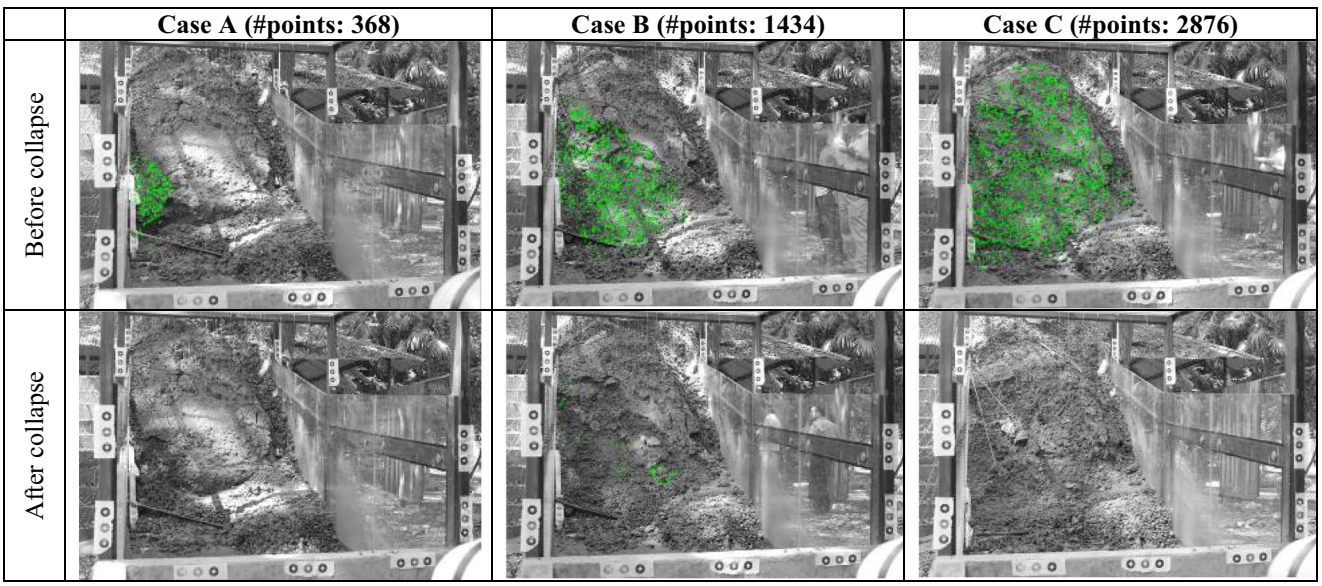

Fig. 8 FPT of an image sequence capturing a scaled-down landslide simulation experiment

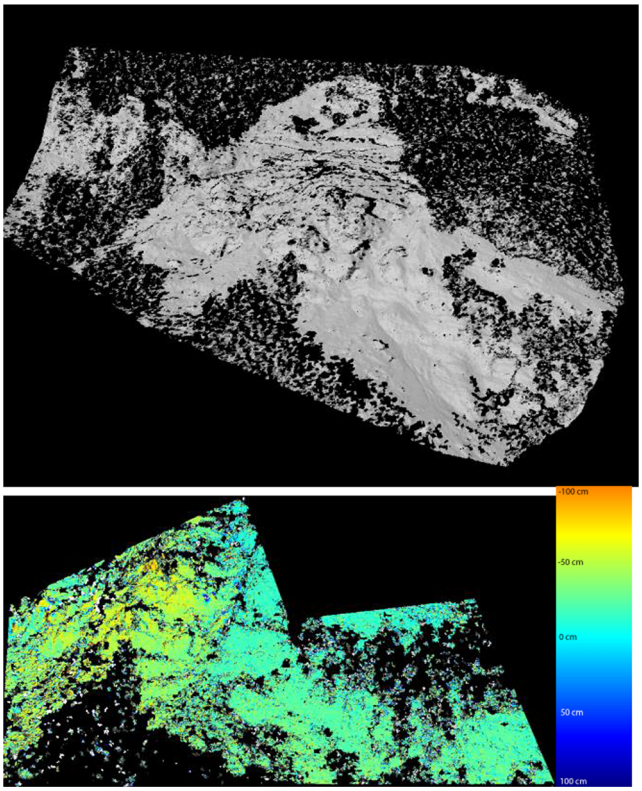

Fig. 9 Results obtained using the stereo-camera system for landslide monitoring

the same time, as deeply described in Roncella et al. (2014), the system must be capable of very good stability along time to avoid the detection of false displacements. For this purpose, an automatic software procedure for checking IO and EO is implemented: whenever a significant variation is encountered, a correction is applied.

In Fig. 9, some results produced by the system are shown. In the top figure, one of the reconstructed DSMs is reported, showing the landslide body in the middle and some vegetated areas around. On the bottom, the displacement map after an observation period of 2 months is shown. The presence of vegetation may result in false ground displacement due to growth during different seasons of the year. To exclude vegetation, first a fixed mask is applied to get rid of lateral regions which are permanently covered by trees. Secondly, the remainder part is analyzed using spatial filtering techniques to detect bushes and other small groups of trees.

Comparison with other monitoring systems (in particular GBSAR, which may provide high-precision observations, see Roncella et al. 2014) shows that the averaged difference between tracked displacements of points in the same areas was 35 mm with a standard deviation of 118 mm.

In addition, such empirical accuracy of the stereo-camera system is in good agreement with the theoretical prediction, even if, with this particular imaging geometry (the cameras are at least 500 m far from the object), noisy results should be expected.

Repeated multi-station networks

The second example concerned the evaluation of large debris movement in the Tartano Valley (Italian Alps). The land erosion in this valley could cause the sediment transport of debris into the Tartano Creek (see Fig. 10). The slope under investigation was 240-m long and 130-m wide. A geodetic network was established to set up a stable GRS to compare measurements at three different epochs. A set of GCPs was placed on the slope and their positions measured with a theodolite. At each epoch, a photogrammetric network made up of 13 images was acquired by using a Nikon D700 camera equipped with a 90-mm lens (see Table 1). This camera was independently calibrated before data acquisition campaigns.

The EO parameters of each block of images were computed by using the automatic procedure ATiPE, see Barazzetti et al. (2010). This outputs a dense set of tie points (see Fig. 10) to be used together with GCPs in the bundle adjustment. In the dense matching stage, the availability of multiple images was exploited to apply the MGCM (Grün and Baltsavias 1988) algorithm described in Previtali et al. (2011) and called MGCM+. Such implementation incorporates techniques to increase the pull-in-range capability and to select the best images to be used for the reconstruction of the different regions of the slope. In a first stage, a DSM with a relative point distance of 15 cm×15 cm was computed. In a second stage, the first DSM was used as input surface to be refined up to a point density of about 2 cm×2 cm.

After the computation of three point clouds describing the ground slope surface at different epochs, a triangulated irregular network (TIN) was derived from each of them. Then, the comparison was carried out by computing volumes between pairs of TIN surfaces. An example of this is reported in the right part of Fig. 10. Considering an estimated precision of about 15 cm, the deformation map does not show a significant modification of the valley topography due, for example, to severe surface erosion. On the other hand, several small areas showing a negative change in the range from −15 to −25 cm were visible, which confirmed the active erosion process. Focusing on some details, some small movements could be observed as well, as proved by the presence of close regions with opposite changes. Unfortunately, the lack of benchmarking data (e.g., from laser scanning) did not allow any validation.

Conclusions

In this paper, an overview on the state-of-the-art image-based deformation measurement (IBDM) has been given along with

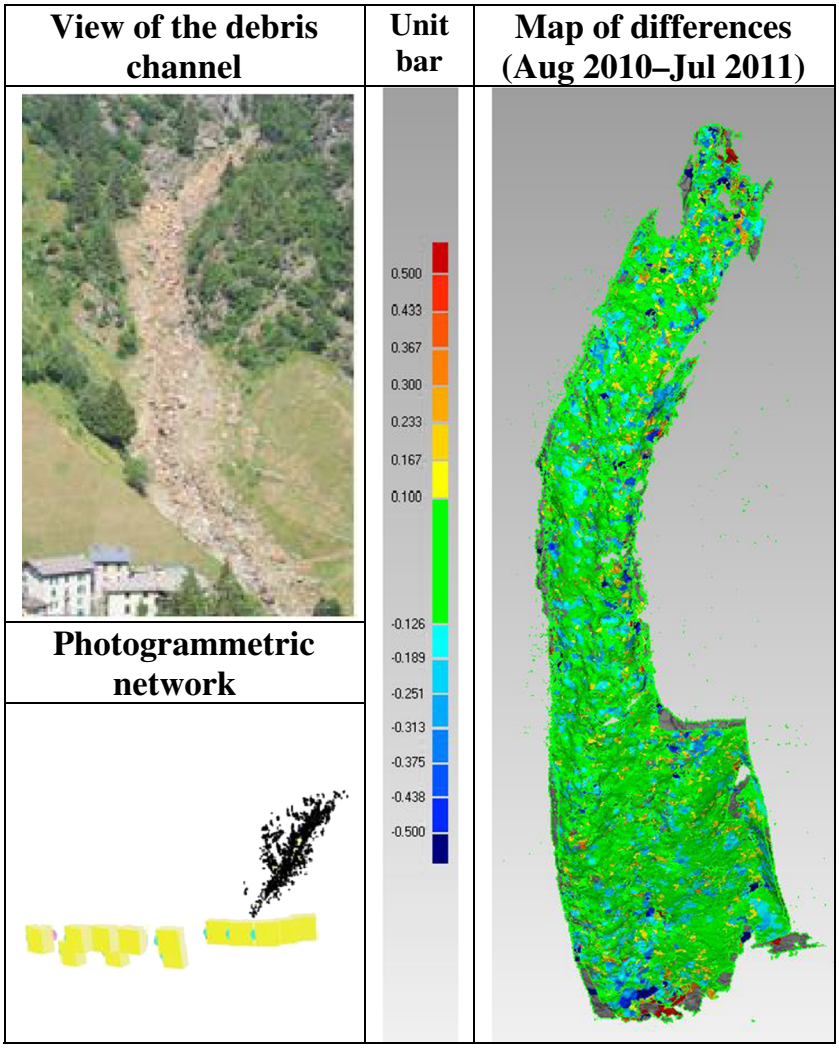

Fig. 10 Results obtained in the multi-epoch comparison of DSMs derived using MGCM+ algorithm in Tartano Valley, Italy (modified from Previtali et al. 2014)

some examples of applications in "Review of IBDM applications."

Different methodologies have been organized into three main categories (see "IBDM methodologies"). The first cate-gory entails the applications based on signalized coded tar-gets, which allow the definition of specific points to be pre-cisely measured and tracked over time ("Applications based on coded targets"). This approach demonstrated to be able to provide precise observations in highly automatic fashion, but it can output only a limited number of tracked points (depend-ing on how many targets are placed). Measurements can be carried out in 2D or 3D, depending on the camera set up.

Surface-point tracking (SPT) based on image matching techniques can be used in order to enlarge the number of points ("Surface-point tracking"). Here two subclasses have been distinguished, depending on the typology of matching algorithm adopted. In the first subclass, area-based matching is used for tracking continuous and regular displacements without sudden changes. In the second subclass (feature-point tracking), feature-based matching offers a major robustness to find corresponding points also when the displacement field is less regular. The approaches in this category are mostly ap-plied for 2D in-plane measurement or for the qualitative evaluation of deformations in the case of non-flat objects. However, SPT is expected to give valuable results also when working with two or more convergent images.

In the third category ("Surface comparison"), the attention is switched on full 3D deformation. Deformation measure-ment is carried out through the reconstruction of the object's surface at any observation epochs by using dense matching techniques. Such surfaces are then compared to detect rigid and non-rigid deformations, as well as loss/accumulation of material. This method has to be followed when changes may happen in a large number of locations in the area under monitoring, like in the case of ground and rock slopes. It can be classified as a real area-based deformation measurement technique, while methods in other categories basically rely on points. The advantage of using the image-based approach mainly consists in the lower cost and in the major transportability and adaptability of cameras with respect to 3D

scanning sensors. However, the integration of different sensors and methods seems an important strategy to be largely exploited in the future.

This research has been partially presented at 2nd Joint International Symposium on Deformation Monitoring in Nottingham (UK), 9–10 September 2013, and co-sponsored by FIG, IAG, and ISPRS.

Acknowledgment This research was partially funded by the National High-Tech R&D Program of China (No. 2012AA121302), the National Basic Research Program of China (No. 2013CB733204), the National Science Foundation of China (No. 41171327), the Specialized Research Fund for the Doctoral Program of Higher Education (No. 20120072120057), and the Italian Ministry of University and Research within the project FIRB2010 (No. RBFR10NM3Z). Many acknowledgements also go to all colleagues and students involved in the organizations of the experiments reported in "Review of IBDM applications." Among others, we would like to thank Prof. L. Binda, Prof. A. Giussani, Dr. Fabio Roncoroni (Politecnico di Milano, Italy), Prof. R. Castellanza (University of Milan Bicocca), Prof. G. Forlani (University of Parma, Italy), Dr. H. Wu, Dr. P. Lu, Prof. R. Li, Prof. X. Tong, and Prof. W. Wang (Tongji University, P.R. China).

References

Apollonio FI, Ballabeni A, Gaiani M, Remondino F (2014) Evaluation of feature-based methods for automated network orientation. Int Arch Photogramm Remote Sens Spat Inf Sci 40(5):47–54

Baker S, Scharstein D, Lewis JP, Roth S, Black MJ, Szeliski R (2011) A database and evaluation methodology for optical flow. Int J Comput Vis 92(1):1–31

Barazzetti L, Scaioni M (2009) Crack measurement: development, testing and applications of an automatic image-based algorithm. ISPRS J Photogramm Remote Sens 64(3):285–296

Barazzetti L, Scaioni M (2010) Development and implementation of image-based algorithms for measurement of deformations in material testing. Sensors 10(8):7469–7495

Barazzetti L, Scaioni M (2011) Photogrammetric tools for deformation measurements. In: 'Proc. XX Congr. Associazione Italiana di Meccanica Teorica e Applicata' (AIMETA), Bologna, Italy, 12–15 Sept. 2011, 10 pages (e-doc online at http://www.lamc.ing.unibo.it/aimeta2011)

Barazzetti L, Remondino F, Scaioni M (2010) Orientation and 3D modelling from markerless terrestrial images: combining accuracy with automation. Photogramm Rec 25(132):356–381

Bay H, Ess A, Tuytelaars T, Van Gool L (2008) Speeded-up robust features (SURF). Comp Vision Image Underst 110(3):346–359

Bethmann F, Luhmann T (2010) Least-squares matching with advanced geometric transformation models. Int Arch Photogramm Remote Sens Spat Inf Sci 38(5):86–91

Bethmann F, Luhmann T (2014) Object-based multi-image semi-global matching—concept and first results. Int Arch Photogramm Remote Sens Spat Inf Sci 10(5):93–100

Birgisson B, Montepara A, Romeo E, Roncella R, Roque R, Tebaldi G (2009) An optical strain measurement system for asphalt mixtures. Mater Struct 42:427–441

Brown DC (1971) Close-range camera calibration. Photogramm Eng 37: 855–866

Dall'Asta E, Roncella R (2014) A comparison of semiglobal and local dense matching algorithms for surface reconstruction. Int Arch Photogramm Remote Sens Spat Inf Sci 40(5):187–194

Fedele R, Scaioni M, Barazzetti L, Rosati G, Biolzi L, Condoleo P (2014) Delamination tests on CFRP-reinforced masonry pillars: optical monitoring and mechanical modelling. Cem Concr Compos 45: 243–254

Feng T, Liu X, Scaioni M, Lin X, Li R (2012) Real-time landslide monitoring using close-range stereo image sequences analysis. In: Proc. '2012 Int. Conf. on Systems and Informatics (ICSAI 2012),' Yantai, P.R. China, 19–21 May 2012, pp. 249–253

Forlani G, Giussani A, Scaioni M, Vassena G (1996) Target detection and epipolar geometry for image orientation in close-range photogrammetry. Int Arch Photogramm Remote Sens Spat Inf Sci 31(B5/V): 518–523

Förstner W, Gülch E (1987). A fast operator for detection and precise location of distinct points, corners and centres of circular features. In Proc. 'ISPRS Intercommission Conf. on Fast Processing of Photogrammetric Data', Interlaken, Switzerland, June 1987, pp. 281–305

Fraser CS (1992) Photogrammetric measurement to One part in a million. Photogramm Eng Remote Sens 58(3):305–310

Fraser CS (1996) Network design. In: Atkinson KB (ed) Close range photogrammetry and machine vision. Whittles, Dunbeath, Caithness, Scotland, pp 256–281

Fraser CS (2013) Automatic camera calibration in close range photogrammetry. Photogramm Eng Remote Sens 79:381–388

Fraser CS, Woods A, Brizzi D (1996) Hyper redundancy for accuracy enhancement in automated close range photogrammetry. Photogramm Rec 20:205–217

Goshtasby A (2005) 2-D and 3-D image registration. John Wiley & Sons, Hoboken, NJ, U.S.A., pp. 258

Granshaw SI (1980) Bundle adjustment methods in engineering photogrammetry. Photogramm Rec 10:181–207

Grün A (1980) Precision and reliability aspects in close range photogrammetry. Int Arch Photogramm Remote Sens 23(B11):378–391

Grün A (1985) Adaptative least squares correlation: a powerful image matching technique. S Afr J Photogramm Remote Sens Cartogr 14: 175–187

Grün A (2012) Development and status of image matching in photogrammetry. Photogramm Rec 27:36–57

Grün A, Baltsavias EP (1988) Geometrically constrained multiphoto matching. Photogramm Eng Remote Sens 54(5):633–641

Haala N (2013) The landscape of dense image matching algorithms. In D Fritsch (Ed.), 'Proc. Photogrammetric Week 2013,' Stuttgart, pp. 271–284

Harris C, Stephens M (1988) A combined corner and edge detector. In: Proc. 'Alvey Vision Conf.,' Vol. 15, 6 pages

Hartley R, Zissermann A (2006) Multiple view geometry in computer vision. Cambridge University Press

Hirschmüller H (2005) Accurate and efficient stereo processing by semi-global matching and mutual information. In: Proc. IEEE Int. Conf. on 'Computer Vision and Pattern Recognition' (CVPR2005), San Diego June 20–26 2005, 8 pages

Hirschmüller H (2008) Stereo processing by semiglobal matching and mutual information. IEEE T Patterns Anal 30(2):328–341

Hoffmann CM (1989) Geometric and solid modeling: an introduction. Morgan Kaufmann Publishers Inc., San Francisco

Jazayeri I, Fraser CS (2010) Interest operators for feature-based matching in close range photogrammetry. Photogramm Rec 25(129):24–41

Lichti DD, Jamtsho S, El-Halawany SI, Lahamy H, Chow J, Chan TO, El-Badry M (2012) Structural deflection measurement with a range camera. J Surv Eng-ASCE 138(2):66–76

Lowe DG (2004) Distinctive image features from scale-invariant keypoints. Int J Comp Vis 60(2):91–110

Luhmann T (2009) Precision potential of photogrammetric 6DOF pose estimation with a single camera. ISPRS J Photogramm Remote Sens 64(3):275–284

Luhmann T (2014) Eccentricity in images of circular and spherical targets and its impact on spatial intersection. Accepted for publication on Photogramm Rec

Luhmann T, Robson S, Kyle S, Boehm J (2013) Close range photogrammetry: 3D imaging techniques. Walter De Gruyter Inc, Germany, p 702

Maas HG (1996) Automatic DEM generation by multi-image feature based matching. Int Arch Photogramm Remote Sens 31(3):484–489

Maas HG, Hampel U (2006) Photogrammetric techniques in civil engineering material testing and structure monitoring. Photogramm Eng Remote Sens 72(1):39–45

Mikolajczyk K, Schmid C (2005) A performance evaluation of local descriptors. IEEE T Patterns Anal 27(10):1615–1630

Mikolajczyk K, Tuytelaars T, Schmid C, Zisserman A, Matas J, Schaffalitzky F, Kadir T, Van Gool L (2005) A comparison of affine region detectors. Int J Comp Vis 65(1–2):43–72

Monserrat O, Crosetto M, Luzi G (2014) A review of ground-based SAR interferometry for deformation measurement. ISPRS J Photogramm Remote Sens 93(1):40–48

Mortenson ME (1985) Geometric modeling. John Wiley & Sons, New York

Niu T, Roque R, Lopp GA (2014) Development of a binder fracture test to determine fracture energy properties. Road Materials and Pavement Design 15(sup1):219–238

Nyce DS (2004) Linear position sensors: theory and application. John Wiley & Sons, New York, p 170

Otepka JO, Fraser CS (2004) Accuracy enhancement of vision metrology through automatic target plane determination. Int Arch Photogramm Remote Sens Spat Inf Sci 35(B5):873–879

Peters WH, Ranson WF (1982) Digital imaging techniques in experimental stress analysis. Opt Eng 21(3):427–431

Previtali M, Barazzetti L, Scaioni M, Tian Y (2011) An automatic multi-image procedure for accurate 3D object reconstruction. In: Proc. '4th Int. Congress on Image and Signal Processing (CISP) 2011,' Shanghai, 15–17 Oct. 2011, Vol. 3, pp. 1400–1404

Previtali M, Barazzetti L, Scaioni M (2014) Accurate 3D surface measurement of mountain slopes through a fully automated image-based technique. Earth Sci Inform 7(2):109–122

Raguse K, Heipke C (2009) Synchronization of image sequences—a photogrammetric method. Photogramm Eng Remote Sens 75(4): 535–546

Remondino F, Del Pizzo S, Kersten TP, Troisi S (2012) Low-cost and open-source solutions for automated image orientation—a critical overview. Springer, Heidelberg, pp 40–54

Remondino F, Spera MG, Nocerino E, Menna F, Nez F (2014) State of the art in high density image matching. Photogramm Rec 29(146): 144–166

Remondino F, Stoppa D (2013) TOF Range-Imaging Cameras. Springer, Berlin Heidelberg

Roncella R, Scaioni M, Forlani G (2004) Application of digital photogrammetry in geotechnics. Int Arch Photogramm Remote Sens Spat Inf Sci 35(B5):93–98

Roncella R, Romeo E, Barazzetti L, Gianinetto M, Scaioni M (2012) Comparative analysis of digital image correlation techniques for in-plane displacement measurements. In: Proc. 5th Int. Congress on 'Image and Signal Processing (CISP2012),' Chongqing, P.R. China, 16–18 Oct. 2012, pp. 721–726

Roncella R, Forlani G, Fornari M, Diotri F (2014) Landslide monitoring by fixed-base terrestrial stereo-photogrammetry. ISPRS Ann Photogramm Remote Sens Spat Inf Sci 2(5):297–304

Rosenfeld A, Kak AC (1976) Digital picture processing (Vol. 1) Elsevier

Rosten E, Drummond T (2006) Machine learning for high-speed corner detection. In: Proc. 'European Conf. on Computer Vision' (ECCV '06) Graz, Austria, 7–13 May 2006, pp. 430–443

Scaioni M, Roncella R, Alba MI (2013a) Change detection and deformation analysis in point clouds: application to rock face monitoring. Photogramm Eng Remote Sens 79(5):441–456

Scaioni M, Lu P, Chen W, Qiao G, Wu H, Feng T, Tong X, Wang W, Li R (2013b) Analysis of spatial sensor network observations during landslide simulation experiments. Eur J Environ Civil Eng 17(9): 802–825

Scaioni M, Feng T, Barazzetti L, Previtali M, Lu P, Giao G, Wu H, Chen W, Tong X, Wang W, Li R (2014a) Some applications of 2D and 3D photogrammetry during laboratory experiments for hydrogeological risk assessment. Geomatics, Natural Hazards and Risk, 24 pages (online at doi:10.1080/19475705.2014.885090)

Scaioni M, Barazzetti L, Giussani A, Previtali M, Roncoroni F, Alba MI (2014b) Photogrammetric techniques for monitoring tunnel deformation. Earth Sci Inf 7(2):83–95

Scharstein D, Szeliski R (2002) A taxonomy and evaluation of dense twoframe stereo correspondence algorithms. Int J C Vis 47(1–3):7–42

Seitz SM, Curless B, Diebel J, Scharstein D, Szeliski R (2006) A comparison and evaluation of multi-view stereo reconstruction algorithms. In: Proc. IEEE Int. Conf. on 'Computer Vision and Pattern Recognition' (CVPR 2006), New York, 17–22 June 2006, Vol. 1, pp. 519–526

Smith SM, Brady JM (1997) SUSAN—a new approach to low level image processing. Int J Comp Vis 23(1):45–78

Spencer L, Shah M (2004) Temporal synchronization from camera motion. In Proc. 6th Asian Conf. on 'Computer Vision,' Jeju Island, Korea, 27–30 January 2004, Vol. 1, pp. 515–520

Szelisky R (2010) Computer vision: algorithms and applications. Springer, Berlin, p 833

Toschi I, Capra A, De Luca L, Beraldin JA, Cournoyer L (2014) On the evaluation of photogrammetric methods for dense 3D surface reconstruction in a metrological context. ISPRS Ann Photogramm Remote Sens Spat Inf Sci 2(5):371–378

Triggs B, McLauchlan P, Hartley R, Fitzgibbon A (2000) Bundle adjustment—a modern synthesis. In: 'Vision Algorithms '99', LNCS No. 1883, Berlin, pp. 298–372

Tuytelaars T, Mikolajczyk K (2008) Local invariant feature detectors: a survey. Found Trends Comput Graph Vis 3(3):177–280

Verhagen B, Timofte R, Van Gool L (2014) Scale-invariant line descriptors for wide baseline matching. In: Proc. IEEE Winter Conference on 'Applications of Computer Vision,' Colorado Springs, CO, USA, 24–26 March 2014, pp. 493–500

Vosselman G, Maas HG (2010) Airborne and terrestrial laser scanning. Whittles, Dunbeath, Caithness, Scotland

Wallis R (1976) An approach to the space variant restoration and enhancement of images. In Proc. Symp. on 'Current Mathematical Problems in Image Science', Naval Postgraduate School, Monterey CA USA, pp. 329–340